Lattice Mean-Field Modeling of Charged Polymeric Micelles

Nadezhda P. Shusharina,*,† Per Linse,† and Alexei R. Khokhlov‡

Physical Chemistry 1, Center for Chemistry and Chemical Engineering, Lund University, P.O.Box 124, S-221 00 Lund, Sweden, and Physics Department, Moscow State University, 117234 Moscow, Russia

Received March 27, 2000; Revised Manuscript Received August 16, 2000

ABSTRACT: Micellization of diblock copolymers with one long and weakly charged and one short uncharged block in an aqueous solution is considered on the basis of a lattice mean-field theory. The critical micellization concentration (cmc) is examined at different fractional charge and length of the hydrophilic block as well as at different solvent quality and salt concentration. Above the cmc, the concentration of free copolymers and the micellar aggregation number are nearly constant. Volume fraction profiles show that the core−corona interface is sharp and that the hydrophilic segments are highly diluted in the corona. The dependences of the micellar aggregation number, the core radius, and corona thickness on several parameters are presented, and they agree qualitatively with scaling predictions. The predictions of the scaling relations are however restricted by the fact of limited scope of micellar stability when a single parameter is varied.

1. Introduction

Micellization in block-copolymer solutions and the structure of the micelles have attracted great interest in recent years.[1−5] Analytic theories for describing the micelle formation of dissolved block copolymers have been developed by many authors.[6−12] In these theories, the blocks are considered to be segregated, forming a completely uniform spherical core made of the lyophobic blocks and an outer shell composed of the lyophilic blocks and the solvent. Often, a simple continuous mean-field approximation is applied to describe the micellar formation and to calculate the free energy of the micelle, and thereafter scaling relations for the equilibrium micellar size are obtained.

The self-consistent mean-field theory developed by Scheutjens and Fleer (lattice version)[13] and by Edwards (continuum version)[14] constitutes another level of description of polymers in heterogeneous systems. The lattice version was adapted by Leermakers et al.[15] to describe surfactant micelle formation and later applied to polymeric micelles by van Lent and Scheutjens[16] and Leermakers et al.[17] Their approach was based on the combination of the thermodynamics of small system developed by Hill[18] with the lattice mean-field theory. Predicted critical micellization concentrations (cmc) and segment density profiles have been found to be in qualitative agreement with experimental data. Extended investigations of the micellization and the micellar structure have been performed by Linse[19,20] and Hurter et al.[21] for models of copolymers containing ethylene oxide and propylene oxide. The temperature dependence of the cmc, the aggregation number, and the hydrodynamic radius were examined on the basis of the lattice mean-field theory extended to copolymers with internal states for describing decreased solubility at increasing temperature.

In the theories mentioned above, uncharged chains were considered throughout. However, many biologically and technically important polymers are charged which produces a richer behavior of the systems. Fundamental investigations of the structural organization of the aggregates made of block copolymers with a charged lyophilic block have been made experimentally.[22−25] Scaling analysis and simple continuous mean-field models have widely been applied to describe the micellization of charged−uncharged diblock copolymers in solutions.[26−30] The conditions for micelle formation and the equilibrium properties of micellar solution including the distribution of the counterions have been considered.

The lattice mean-field theory was extended to charged molecules by Böhmer et al.[31] and by Israels[32] and applied to study the adsorption of weakly charged polyelectrolytes at planar and oppositely charged surfaces.[33,34] Planar polyelectrolyte brushes[35] and star-branched polyelectrolytes[36] have also been considered by this method. The general trends predicted earlier on the basis of a scaling approach[37−40] have been confirmed by lattice mean-field results.

In our previous publication,[41] we have presented an extended scaling description of the equilibrium properties of an individual micelle with a lyophobic spherical core and a charged corona. A diagram with different regimes of the behavior of micellar properties has been constructed. We also used the lattice mean-field approach to model the micellar structure in the regimes of quasi-planar corona geometry. Specifically, we considered polyelectrolyte chains grafted to a spherical surface of large radius in comparison with the length of the chains. This system corresponds to the case of so-called "crew-cut" micelles for which the aggregation number and the core radius depends only on the length of lyophobic block. The calculated dependence of the corona thickness on the length and the charge of the grafted chains was consistent with the scaling predictions.

In the present paper we consider the equilibrium behavior of an individual micelle in aqueous solution composed of diblock copolymers with charged hydrophilic blocks in the framework of the lattice self-consistent mean-field approach. Contrary to the case considered in ref 41, we now treat the more general case where the aggregation number and the core radius depends on the properties of the hydrophilic block as well. Our aim is to model the cmc and the structure of

† Lund University.
‡ Moscow State University.

10.1021/ma0005567 CCC: $19.00
Published on Web 10/07/2000

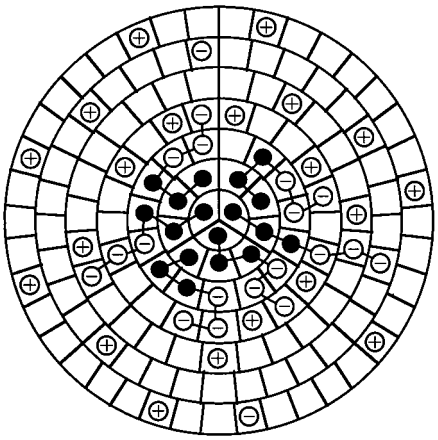

Figure 1. Two-dimensional illustration of an infinite spherical lattice and a micelle formed by six diblock copolymers. The uncharged hydrophobic segments (filled circles) form the central part of the micelle, whereas the charged and more hydrophilic segments (connected open circles) form the outer layer of the micelle. Anions and cations are also given (unconnected open circles). Note the small number of unfavorable contact between the hydrophobic segments and the solvent (unfilled lattice cells).

"hairy" micelles, i.e., micelles with a large corona as compared to the core. We will also compare the numerical results with analytical scaling predictions.

2. Method

2.1. Theoretical Model. We will here present only the main features of the lattice mean-field theory for the self-assembly of charged block copolymers adapted to our study; for further details the reader is referred to the original publications.[13,16,17,31,32] Briefly, the space is divided into spherical shells, $i = 1, 2, ...$, and each shell is further divided into lattice cells of equal volume. The conformations of a polymer chain are described as random walks on the spherical lattice. Within each shell the Bragg−Williams approximation of random mixing is applied, and thus all sites in a shell are equivalent. Each lattice cell contains either one polymer segment, one solvated ion, or solvent (water). The model contains five different species: negatively charged polymer segments, uncharged polymer segments, cations, anions, and solvent. At concentrations above the critical micellization concentration there will be one polymer micelle located at the center of the spherical lattice (see Figure 1).

Since within each layer a mean-field approximation is applied, we can write the volume fraction profiles of the species as functions of layer number i only. The possibility of obtaining radial concentrations profiles is coupled to the existence of radial dependent potentials. The species potential u_{Si} is determined as the derivative of the free energy with respect to the species concentration. The potential is species dependent and is defined to be zero in a homogeneous bulk solution far away from the center of the lattice (micelle). The species potential can be expressed as a sum of three terms according to

$$u_{Si} = u_i' + u_{Si}^{\mathrm{int}} + u_{Si}^{\mathrm{el}} \tag{1}$$

where u_i' is a "hard-core" contribution, u_{Si}^{int} a contribution from short-range interactions, and u_{Si}^{el} a contribution from long-range Coulomb interactions. The species-independent term u_i' ensures that the space is completely filled in layer i according to $\sum_S \phi_{Si} = 1$, $i = 1, 2, ...$, where ϕ_{Si} is the volume fraction of species S in layer i. The value of u_i' is related to the lateral pressure in a continuous model, and in bulk u_i' becomes zero. The short-range contribution u_{Si}^{int} is expressed by

$$u_{Si}^{\mathrm{int}} = k_{\mathrm{B}}T\sum_{S'}\chi_{SS'}(\langle\phi_{S'i}\rangle - \phi_{S'}^{\mathrm{b}}) \tag{2}$$

where $\chi_{SS'}$ is Flory−Huggins interaction parameter for the $S-S'$ pair,[42] k_{B} is Boltzmann's constant, and T is the temperature. In eq 2, the angular brackets denote an averaging over three adjacent layers, and $\phi_{S'}^{\mathrm{b}}$ is the free (bulk) volume fraction of species S'. In bulk, $u_{Si}^{\mathrm{int}} = 0$. Finally, the long-range Coulomb interaction energy is given by

$$u_{Si}^{\mathrm{el}} = q_S\Psi_i \tag{3}$$

where q_S is the charge of species S and Ψ_i the electrostatic potential of mean force in layer i. In line with the random mixing approximation of the short-range interaction, it is reasonable to let the electrostatic potential depend only on the radial distance. Moreover, we assume (arbitrarily) $\Psi^{\mathrm{b}} = 0$. We relate the potential of mean force to the charge density through Poisson's equation

$$\epsilon_0\epsilon_{\mathrm{r}}\nabla^2\Psi_i = -\rho_i \tag{4}$$

where $\epsilon_0\epsilon_{\mathrm{r}}$ is the dielectric permittivity of the medium, ∇^2 is the Laplacian, and $\rho_i = \sum_S q_S\phi_{Si}$ the charge density in layer i. The charges of the species are located to spherical surfaces in the middle of each lattice shell, and the space between the charged surfaces is free of charge. To calculate the volume fraction of a species in layer i, it is convenient to introduce weighting factors, which are Boltzmann weights of the species potentials according to

$$G_{Si} = \mathrm{e}^{-u_{Si}/k_{\mathrm{B}}T} \tag{5}$$

If u_{Si} and thus G_{Si} are known, the relative weight of all the possible conformations can be calculated, and hence also the volume fraction profiles can be evaluated. The species volume fraction ϕ_{Si} is simply related to n_{xsi}, the number of sites in layer i occupied by segments of rank s (the sth segment in a chain) belonging to component x according to

$$\phi_{Si} = \frac{1}{L_i}\sum_x\sum_{s=1}^{N_x}\delta_{S,t(x,s)}n_{xsi} \tag{6}$$

where L_i is the number of lattice sites in the layer i, and N_x is the number of segments forming the molecule in component x ($N_x = 1$ for salt and water and $N_x > 1$ for the polymer). The Kronecker δ selects only segments of rank s of component x if they are of type S.

The expression for the segment distribution is more complex. The correct weights of all conformations, as well as the connectivity of the chains, have to be taken into account. With the partition function as origin, n_{xsi} is obtained by the use of a matrix method and is then given by[43]

$$n_{xsi} = C_x\{\Delta_i^T\cdot[\prod_{s'=N_x}^{s+1}(\mathbf{W}^{t(x,s')})^T]\cdot\mathbf{s}\}\{\Delta_i^T\cdot[\prod_{s'=2}^{s}\mathbf{W}^{t(x,s')}]\cdot\mathbf{p}(x,1)\} \quad (7)$$

where C_x is a normalization factor related to the bulk volume fraction of component x, $\mathbf{W}^{t(x,s')}$ is a tridiagonal matrix comprising elements which contains factors describing the lattice topology as well as weighting factors for each segment of rank s belonging to component x, and $\mathbf{p}(x,1)$ is a vector describing the distribution of the first segment of component x among the layers, Δ and $\mathbf{s}$ being elementary column vectors. Since u_{Si} is needed for obtaining ϕ_{Si} using eqs 5−7 and since u_{Si} depends in turn on ϕ_{Si} according to eqs 1 and 2, eqs 1, 2, and 5−7 need to be solved self-consistently. In addition the electrostatic potential, which enters in eq 1 via eq 3, has to fulfill Poisson's equation, eq 4.

2.2. Micelle Formation. The numerical solution of eqs 1−7 can be of two kinds: one corresponding to homogeneous concentration profiles throughout the entire lattice and one to a single micelle formed at the center of the lattice and in equilibrium with specified bulk concentration of the components. In the latter case, the excess free energy of the micelle with respect to the free energy in the bulk solution is of great importance. The thermodynamics of small system developed by Hill[18] is useful to study the equilibrium conditions of the micellar solution. In this approach, the solution is divided into subsystems of volume V_s, which contain one micelle and accompanying solution. The excess free energy of the subsystem A^{exc} can be written as a sum of two contributions:[16]

$$A^{exc} = A^{\sigma} + k_B T \ln(V_m/V_s) \quad (8)$$

where V_m is the volume of a micelle. The first term is the free energy necessary to create a micelle with fixed center of mass, whereas the second one is the mixing entropy of the micelles. A^{σ} is readily calculated from (i) the volume fraction distributions of the species and (ii) the chemical potentials of the components in bulk according to eqs 2−5, 14, and 15 in ref 19, augmented with electrostatic contributions. At equilibrium, A^{σ} is balanced by a negative contribution from the mixing entropy $k_B T \ln(V_m/V_s)$.

The excess number of polymer segments in the subsystem is defined as

$$\Gamma_p = \sum_{i=1}^{M} L_i[(\sum_{s=1}^{N_p}\phi_{psi}) - \phi_p^b] \quad (9)$$

where $\phi_{psi} = n_{psi}/L_i$ and ϕ_p^b is the bulk polymer volume fraction. The micellar aggregation number N_{agg} is the excess number of polymer molecules in the subsystem given by

$$N_{agg} = \Gamma_p/N_p \quad (10)$$

As the polymer volume fraction in the micellar core is nearly constant, the micellar volume is approximated by

$$V_m = \frac{\Gamma_p}{\phi_{p,i=1} - \phi_p^b} \quad (11)$$

Table 1. Parameters of the Model

quantity	value
temperature	$T = 298$ K
relative dielectric permittivity	$\epsilon_r = 80$
lattice spacing	$d = 7$ Å
degree of polymerization	$N_A = 130-300$
	$N_B = 30$
fractional segment charge	$\tau = 0-0.01$
salt volume fraction	$\phi_s = 0-0.001$
interaction parameters[a]	$\chi_{AB} = 0.5$
	$\chi_{AW} = 0, 0.5$
	$\chi_{BW} = 1.8$

[a] Other interaction parameters are zero.

The total volume fraction of the polymer in the subsystem (equal to the stoichiometric polymer concentration in the micellar solution) is the sum of the excess and bulk volume fractions according to

$$\phi_p^{tot} = \Gamma_p/V_s + \phi_p^b \quad (12)$$

Generally, the concentration at which micelles experimentally start to be observable is referred to as the cmc. In this model, this corresponds to stating that the cmc is the polymer volume fraction at which A^{σ} attains its maximum as a function of the micellar aggregation number in the volume fraction interval where a numerical solution representing a thermodynamically stable inhomogeneous system exists.

In practice, the calculations are performed by initially fixing the bulk polymer volume fraction ϕ_p^b (or equivalently its chemical potential). From the volume fraction profiles we obtain the excess number of polymer segments Γ_p and the excess free energy A^{σ}. Thereafter, the micellar aggregation number and the volume of the micelle are calculated from eqs 9−11. By taking into account the equilibrium condition $A^{exc} = 0$ (see eq 8), the volume of the subsystem V_s is subsequently determined. Finally, from eq 12 the total polymer concentration ϕ_p^{tot} is calculated.

2.3. Model System and Parameters. The five species of our model are referred to as (A) negatively charged polymer segment, (B) uncharged polymer segment, (C) cation, (D) anion, and (W) solvent. The diblock copolymer is considered to be completely flexible consisting of N_A charged segments, each carrying the fractional charge $-|e|\tau$ and N_B uncharged segments. Hence, we have a smooth charge distribution of the charged block and in total τN_A charges per polymer. The small ions are throughout monovalently charged.

The values of the parameters in our study are compiled in Table 1. Typically, the micelle is composed of diblock copolymers $A_{300}B_{30}$ with a fractional charge $\tau = 0.01$ of the A-segments. The charged and uncharged polymer segments displays a short-range repulsion ($\chi_{AB} = 0.5$), the solvency of the charged block is either athermal ($\chi_{AW} = 0$) or Θ-like ($\chi_{AW} = 0.5$), and the uncharged block is strongly hydrophobic ($\chi_{BW} = 1.8$), whereas the other interaction parameters are zero for simplicity.

A lattice spacing of 7 Å is selected, and at the given conditions it is approximately equal to the Bjerrum length $l_B = e^2/(4\pi\epsilon_0\epsilon_r k_B T)$. The choice $\tau \ll 1$ makes neighboring charges along the chain only weakly coupled. The lattice is composed of $M = 200$ radial layers, and reflecting boundary conditions are chosen at the pe-

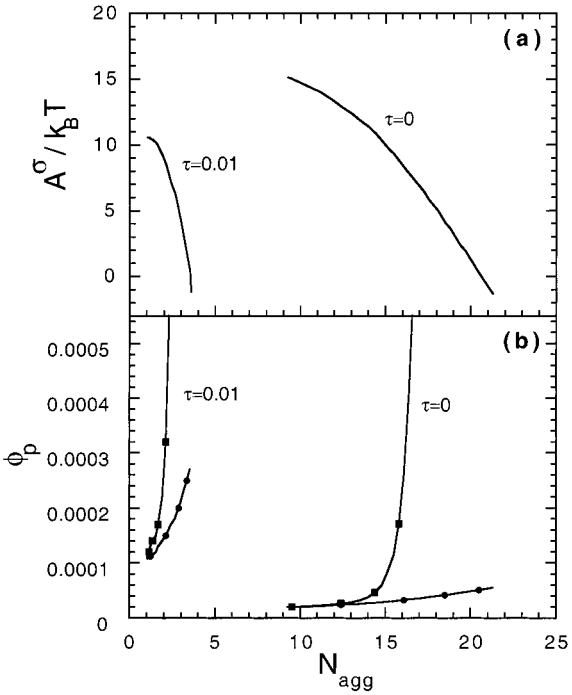

Figure 2. (a) Excess free energy and (b) bulk (circles) and total (squares) polymer volume fraction vs the aggregation number of the micelle composed of $A_{300}B_{30}$ molecules for uncharged and charged A-segments with the fractional charge $\tau = 0.01$ at athermal solvent condition ($\chi_{AW} = 0$).

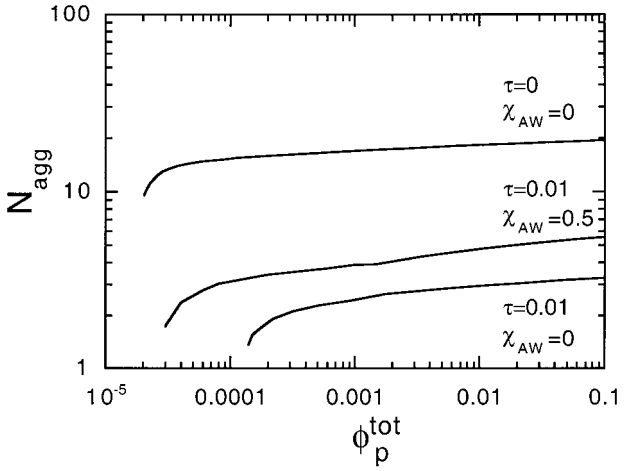

Figure 3. Aggregation number of micelles composed of $A_{300}B_{30}$ copolymers vs the total polymer volume fraction at indicated fractional charge of the A-segments and solvency condition.

riphery of the lattice, i.e., $\phi_{S,201} = \phi_{S,200}$ and $u_{S,201} = u_{S,200}$ for all S.

3. Results

3.1. Micellar Stability and the Cmc. Initially, we will illustrate the computational approach by examine the stability of micelles formed by diblock copolymers with uncharged or charged hydrophilic blocks. In Figure 2a, we present the excess energy A^σ as a function of the micellar aggregation number N_{agg} as obtained by repeated calculations for different ϕ_p^b. The maximum of $A^\sigma(N_{agg})$ corresponds to the minimum aggregation number which the micelles attain at their cmc. On the left-hand side of the maximum, stable micelles do not exist; practically, it means that there is no numerical solution. (Formally, the curve should end with a zero slope, but

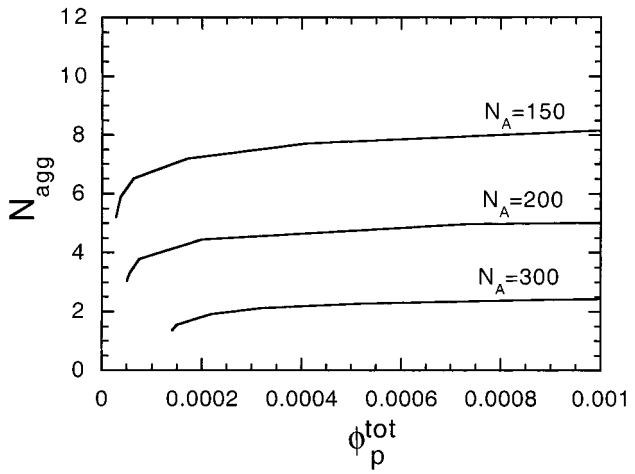

Figure 4. Aggregation number of micelles composed of $A_{N_A}B_{30}$ copolymers vs the total polymer volume fraction at indicated A-block length with the fractional charge $\tau = 0.01$ of the A-segments and at athermal solvent condition ($\chi_{AW} = 0$).

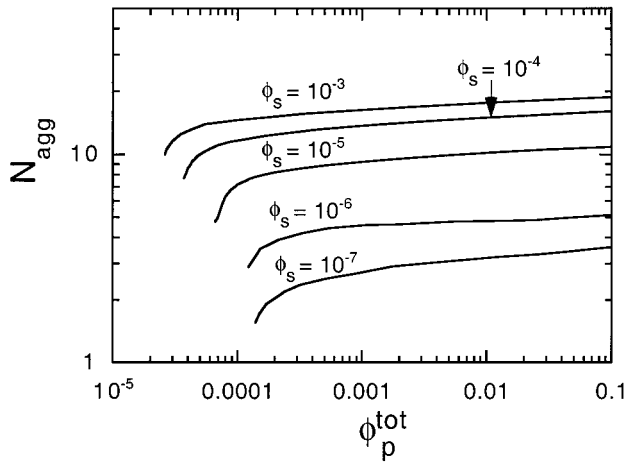

Figure 5. Aggregation number of micelles composed of $A_{300}B_{30}$ copolymers vs the total polymer volume fraction at indicated volume fraction of monovalent salt with the fractional charge $\tau = 0.01$ of the A-segments and at athermal solvent condition ($\chi_{AW} = 0$).

numerical difficulties prohibit a solution in close proximity to the cmc.) The right-hand side of the maximum corresponds to stable aggregates. The micelles grow and are thermodynamically stable until other nonspherical aggregate shapes becomes thermodynamically favored. The determination of this transition requires additional calculations with other geometries.[44]

In Figure 2b, we show the corresponding dependence of the bulk polymer volume fraction ϕ_p^b and the total polymer volume fraction ϕ_p^{tot} on the micellar aggregation number. Recall that these relationships are generated by subsequent calculations with varying ϕ_p^b. The lower end of the ϕ_p^b and ϕ_p^{tot} curves corresponds to the maximum in A^σ. The much more rapid increase of ϕ_p^{tot}, as compared to ϕ_p^b, at increasing N_{agg} shows that the bulk volume fraction (or equivalently the chemical potential) of the polymer increases only weakly after the cmc.

Figures 3−5 show the micellar aggregation number N_{agg} as a function of the total polymer volume fraction ϕ_p^{tot} with different properties as parameters. In contrast to ϕ_p^b, ϕ_p^{tot} is directly experimentally accessible, and N_{agg} is a property often determined. Common to all

cases considered, the aggregation number increases only weakly at increasing total polymer volume fraction above the cmc. Typically, N_{agg} increases by a factor of 2 when ϕ_p^{tot} increases by 3 orders of magnitude. However, near the cmc, N_{agg} displays a stronger dependence on ϕ_p^{tot}.

In Figure 3, we display the results for uncharged and charged A-blocks at athermal solvent condition ($\chi_{AW} = 0$) and for the same charged A-block at Θ-condition ($\chi_{AW} = 0.5$). Considering the effects of charges first, we find that the introduction of the charges reduces the aggregation number from ca. 10−20 to 2−3 and increases the cmc by a factor of 10. For the charged diblock copolymer, the worsening of the solvent condition from $\chi_{AW} = 0$ to 0.5 leads to an increase of the aggregation number from 2−3 to 3−6 and a reduction of the cmc by a factor of 5. Thus, the micellization is facilitated by a worsening of the solvency condition of the hydrophilic block but is disfavored by introducing charges on the hydrophilic block. The present results obtained for salt-free solutions indicates that even small amount of charges have a significant effect. Here, each A-block carries only three elementary charges.

The corresponding N_{agg} dependence on ϕ_p^{tot} at different number of segments of the charged block at otherwise constant conditions are shown in Figure 4. An increase of N_A from 150 to 300 leads to a reduction of the aggregation number from ca. 8 to ca. 2, whereas the cmc rises by a factor of 8. Thus, an increase of the length of the hydrophilic charged block promotes smaller micelles and higher cmc.

In Figure 5, the same dependence at different addition of monovalent salt in the range $\phi_s = 10^{-7}-10^{-3}$ is displayed. The smallest micelles are found at the lowest salt concentration, whereas at $\phi_s = 10^{-3}$ the electrostatic screening is nearly complete. The results for charged micelles at $\phi_s = 10^{-3}$ and for uncharged micelles are nearly the same (cf. curve labeled $\phi_s = 10^{-3}$ in Figure 5 and curve labeled $\tau = 0$, $\chi_{AW} = 0$ in Figure 3).

3.2. Micellar Structure. The radial density distributions of the different species appear as a result of the lattice mean-field theory; hence they are not preassumed as often in more simplified theories. In Figure 6, we show various radial volume fraction profiles for a micelle formed by $A_{300}B_{30}$ copolymers with a fractional charge $\tau = 0.01$ of the A-segments at athermal solvent condition and a salt volume fraction $\phi_s = 10^{-4}$. We have selected a total volume fraction ϕ_p^{tot} giving $N_{agg} = 15$.

Figure 6a shows the radial volume fraction profiles of the two types of polymer segments and the solvent. For our very asymmetric block copolymer, we find a relatively small core with a high volume fraction of the hydrophobic B-segments and little solvent. The micellar core is surrounded by a very extensive corona of highly solvated A-segments. It is preferable to describe the interface between the B-rich core and the corona as a border between B-segments and solvent, owing to the high dilution of the A-segments. The location of the interface appears at layer $i \approx 5$ (the layer where $\phi_{Bi} \approx \phi_{Wi}$) and the interface is relatively sharp owing to the high χ parameter between B-segments and the solvent ($\chi_{BW} = 1.8$).

As shown by eq 7, the lattice theory also provides volume fraction profiles of segments of given rank. In Figure 6b, the volume fraction profiles of the A-end segments, the B-end segments, and the AB-junctions are shown. We see that the distribution of the A-ends is very

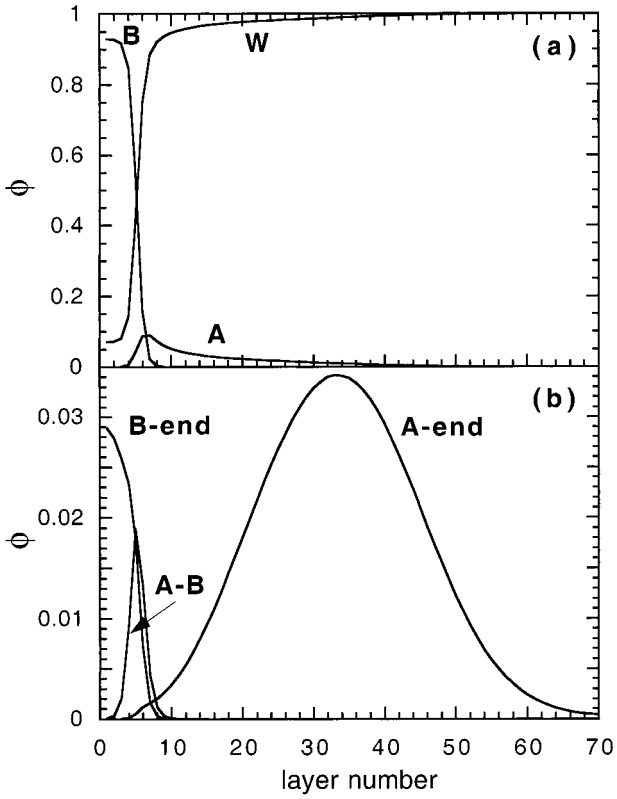

Figure 6. Radial volume fraction profiles (a) of A-segments (A), B-segments (B), and water (W) and (b) of A-end segments (A-end), B-end segments (B-end), and AB-junctions (A-B) of a micelle composed of $A_{300}B_{30}$ copolymers with the fractional charge $\tau = 0.01$ of the A-segments and at athermal solvent condition ($\chi_{AW} = 0$) and salt volume fraction $\phi_s = 10^{-4}$. $\phi_p^{tot} = 0.01$. In (b), the A-end curve is multiplied by 1000.

broad and Gaussian-like with a peak in layer $i \approx 34$, whereas the volume fraction of the B-ends follow closely the distribution displayed of all B-segments. The distribution of the AB-junctions is narrow, and naturally, its volume fraction peaks at the core−corona interface.

The volume fraction profiles of the charged species at the same conditions as in Figure 6 but with different volume fractions of added salt are given in Figure 7 on a semilogarithmic scale. Here, the profiles for the A-segments are multiplied by τ. A comparison among the profiles of the A-segments shows that the larger aggregation number occurring at higher salt concentration (see Figure 5) leads to a profile shifted outward and having a slightly larger magnitude. Moreover, their slope in the part of the corona close to the maximum ($8 < i < 25$) decreases with increasing salt concentration. Figure 7 shows also that the difference between volume fraction of counterions (labeled as C) and co-ions (labeled as D) is the largest at the peak of ϕ_{Ai} and that the difference becomes smaller as the salt concentration increases. At increasing layer number, the counterion and co-ion profiles approach each other and eventually they attain their common bulk value.

Consider now the charge integrated up to a given layer i according to

$$Q_i = \sum_{i'=0}^{i} \sum_{S} q_S \phi_{Si'} \tag{13}$$

i.e., the net charge within a sphere of radius i. The ratio of Q_i and the absolute value of the micellar charge Q_{mic}

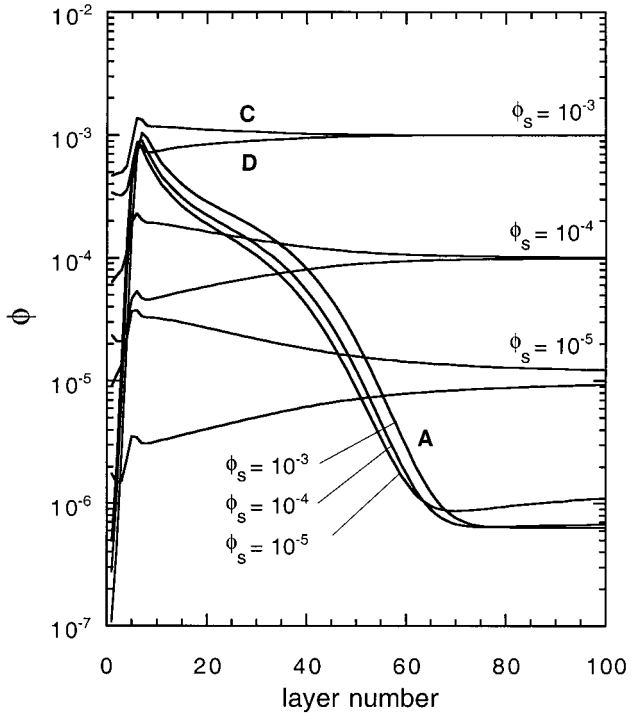

Figure 7. Radial volume fraction profiles of A-segments (A), cations (C), and anions (D) of a single micelle composed of $A_{300}B_{30}$ copolymers with a fractional charge $\tau = 0.01$ of the A-segments and at athermal solvent condition ($\chi_{AW} = 0$) and indicated salt volume fraction. The volume fraction profiles of the A-segments are multiplied by τ.

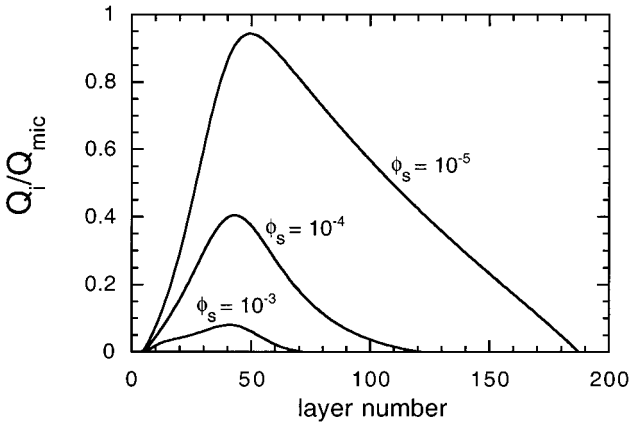

Figure 8. Integrated charge divided by the micellar charge Q_i/Q_{mic} (see text) at indicated salt volume fractions. The conditions are the same as in Figure 7.

$= |e|\tau N_A N_{agg}$ for micelles formed in solutions at the different salt volume fractions are shown in Figure 8. In all cases, the fractional charge increases in the inner region of the corona, reaches a maximum at $i \approx 40-50$, and reduces to zero due to compensating counterions at larger distance. The maximum of Q_i/Q_{mic} is the maximal fraction of uncompensated micellar charge appearing at some radial distance. At the lowest salt concentration $\phi_s = 10^{-5}$, the maximal Q_i/Q_{mic} is close to one, signaling a prominent double layer, whereas at the highest salt concentration $\phi_s = 10^{-3}$ the distribution is nearly uniform with the maximum $Q_i/Q_{mic} \approx 0.1$. At $\phi_s = 10^{-4}$ we have an intermediate situation. Moreover, the decay to zero is much faster at the higher salt volume fraction owing to the improved electrostatic screening.

Thus, the picture emerging is that at low salt concentration we have an extended electrical double layer and an appreciable difference in the counterion and coion volume fractions extending far beyond the distances at which the hydrophilic A-block has attained its bulk concentration. At increasing salt concentration, the double layer is reduced in magnitude and extension, and it becomes located inside the corona. At the highest salt concentration, the diblock copolymer micelle and the ions embedded in the corona constitute a neutral object.

3.3. Comparison with Scaling Approaches. We will now in more detail examine the dependences of the aggregation number N_{agg}, the corona thickness R_A, and the core radius R_B on the fractional charge τ of the A-segments, the length N_A of the A-block, and the salt volume fraction ϕ_s. In particular, we will compare these dependences with those given by a scaling approach. All the numerical results have been obtained for a total polymer volume fraction $\phi_p^{tot} = 0.01$, and of course the cmc varies widely as τ, N_A, or ϕ_s is changed. Therefore, we cannot always vary τ or N_A over a sufficiently large range to predict power laws. Thus, in some cases we are restricted to assess whether the results of the lattice mean-field model are qualitatively consistent with the scaling predictions.

In this analysis, the corona thickness R_A was evaluated as the second moment of the volume fraction profile of the A-end segments of the diblock copolymers starting from $i = i_{core} = R_B$ according to

$$R_A = \left(\frac{\sum_{i=i_{core}}^{M} \phi_{end,i}(i - i_{core})^2}{\sum_{i=i_{core}}^{M} \phi_{end,i}} \right)^{1/2} \qquad (14)$$

The location of the maximum of the A-segments volume fraction profile is taken as the border between the corona and the core and hence as the radius of the core R_B (see Figure 6a). The outcome is not sensitive on the precise definition of R_B.

Figure 9 shows N_{agg}, R_A, and R_B as a function of τ at athermal ($\chi_{AW} = 0$) solvent condition and $N_A = 300$. We see that the aggregation number and the core radius decrease, whereas the corona thickness increases with increasing fractional charge of the A-segments. Further analysis gives the power dependences $N_{agg} \sim \tau^{-1.2}$, $R_A \sim \tau^{0.1}$, and $R_B \sim \tau^{-0.2}$. Owing to $N_A \gg N_B$ and that most counterions are outside the corona, we expect that the behavior of the system is primarily consistent with the spherical Pincus brush regime of the different scaling regimes presented in ref 41. For the spherical Pincus brush regime, the scaling theory predicts $N_{agg} \sim \tau^{-15/11}$, $R_A \sim \tau^{2/11}$, and $R_B \sim \tau^{-5/11}$, whereas in the neighboring quasi-neutral regime all properties are independent of τ and in the remaining neighboring regimes the τ dependence is stronger than in the spherical Pincus regime. The perfect scaling behaviors over a 5-fold change in τ and the close relation between the power laws found and those for the Pincus regime suggest that the present lattice modeling confirm the existence of the spherical Pincus brush regime.

In Figure 10, the dependences of N_{agg}, R_A, and R_B on N_A at athermal solvent condition and charged ($\tau = 0.01$) and uncharged ($\tau = 0$) hydrophilic block are displayed. Qualitatively, the aggregation number and the core

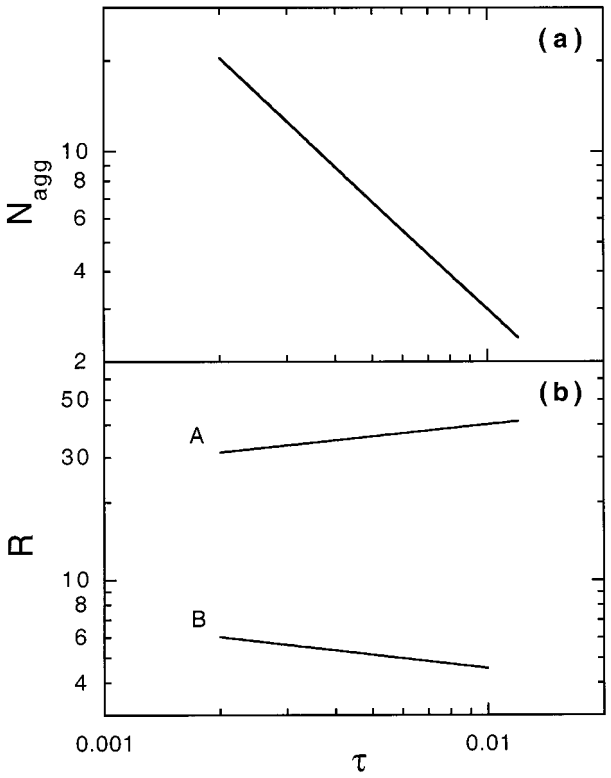

Figure 9. (a) Aggregation number and (b) corona thickness (A) and core radius (B) of micelles composed of $A_{150}B_{30}$ diblock copolymers vs fractional charge τ of the A-segments at $\phi_p^{tot} = 0.01$ and athermal solvent condition ($\chi_{AW} = 0$).

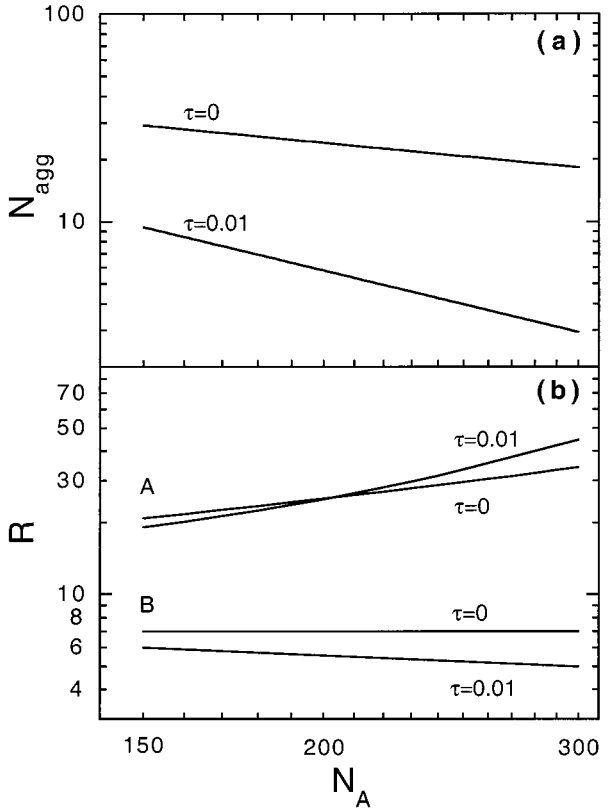

Figure 10. (a) Aggregation number and (b) corona thickness (A) and core radius (B) of micelles composed of $A_{N_A}B_{30}$ diblock copolymers vs the length of the A-block with indicated fractional charge of the A-segment at $\phi_p^{tot} = 0.01$ and athermal solvent condition ($\chi_{AW} = 0$).

radius decrease, whereas the corona thickness increases with increasing length of the hydrophilic block. In more detail, we have $N_{agg} \sim N_A^{-1.6}$, $R_A \sim N_A^1$, and $R_B \sim N_A^{-0.3}$ at $\tau = 0.01$ and $N_{agg} \sim N_A^{-0.7}$, $R_A \sim N_A^{0.85}$, and $R_B \sim N_A^0$ at $\tau = 0$. The corresponding scaling predictions in the spherical Pincus brush regime are $N_{agg} \sim N_A^{-21/22}$, $R_A \sim N_A^{8/11}$, and $R_B \sim N_A^{-7/22}$, whereas the corresponding scaling predictions in the quasi-neutral regime are $N_{agg} \sim N_A^0$, $R_A \sim N_A^{3/5}$, and $R_B \sim N_A^0$. A comparison between the power laws predicted by the lattice mean-field model and by the scaling approach shows that (i) the difference in the exponents between the lattice and the scaling approach of a given property is the same for $\tau = 0$ and $\tau = 0.01$ and (ii) the difference amounts to -0.7 for the N_{agg} dependence, 0.3 for the R_A dependence, and <0.1 for the R_B dependence. The very good agreement of the predicted R_A and R_B dependencies on N_A for both regimes suggests that we again have identified the matching scaling regimes to our numerical lattice results. However, regarding the dependence of N_{agg} on N_A the difference between the two approaches is considerable. Since the same disagreement appears for both charged and uncharged hydrophilic blocks, it is not likely due to different treatment of the Coulomb interaction. One possible explanation could be the fact that the scaling theory assumes a uniformly and completely filled core ($\phi_B = 1$), whereas in the lattice mean-field theory $\phi_B < 1$ and ϕ_B varies according to the conditions. For example, Figure 6a shows that the B-rich core is slightly solvated. An increasing length of the hydrophilic A-block leads to an increasing amount of solvent in the core, making the aggregation number to decay faster than predicted by scaling.

Finally, the influence of monovalent salt on the equilibrium size characteristics of the micelles is shown in Figure 11. The addition of simple salt up to some concentration does not influence the micellar size. In this regime, the electrostatic screening of the charged A-segments is dominated by the counterions of the copolymer. However, an increase of ϕ_s above a certain threshold results in an increase of the micellar aggregation number as well as the core radius, whereas the corona thickness is decreased. The corresponding power dependences are $N_{agg} \sim \phi_s^{0.35}$, $R_A \sim \phi_s^{-0.06}$, and $R_B \sim \phi_s^{0.03}$. The very weak dependences of the corona thickness and the core radius are noticeable. At even higher salt concentration the effects level off and the properties of the micelle approaches that for those formed by corresponding uncharged copolymer. This behavior is in a qualitative agreement with the scaling predictions by Borisov and Zhulina.[45] According to them, there are salt-independent regimes at low and high salt concentrations, and two intermediate regimes in which the aggregation number increases, while the radius of the micellar corona weakly decreases as a function of the salt concentration. The corresponding exponents are 6/11 and 3/5 for the aggregation number and $-1/11$ and $-2/25$ for the corona size, respectively. Because of the very small difference in the values of the exponents in two salt-dependent regimes, they are not likely to be distinguishable either in numerical modeling or experimentally.

4. Discussion

Generally, the strong unfavorable interaction between the hydrophobic segments and water is the driving force of the micellization of diblock copolymers in a selective

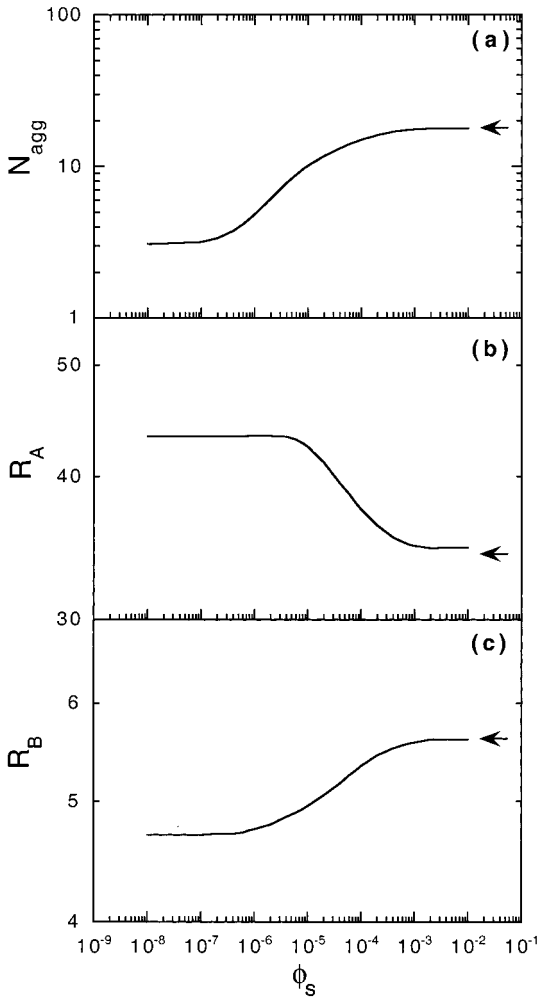

Figure 11. (a) Aggregation number, (b) corona thickness, and (c) core radius of micelles composed of $A_{150}B_{30}$ diblock copolymers vs the volume fraction of monovalent salt with the fractional charge $\tau = 0.01$ of the A-segments and at $\phi_p^{tot} = 0.01$ and athermal solvent condition ($\chi_{AW} = 0$). The horizontal arrows show the results for the corresponding uncharged diblock copolymers in the absence of salt.

solvent, whereas there are several mechanisms limiting the micellar growth. For "hairy" micelles, as considered here, the effective repulsion among the hydrophilic blocks in the corona is normally the dominating factor restricting the micellar growth. Our numerical results clearly support this picture. The reduction of the aggregation number at an increase of the length of the hydrophilic block constitutes direct evidence of that. The accompanying reduction of the core size is just a reflection of the combined effect of the reduction of the aggregation number and the compactness of the core. In contrast, the corona thickness increases despite the reduction of the aggregation number; hence, the increase of the length of the hydrophilic block and its stretching have a larger influence than the reduction of the aggregation number on the corona thickness.

Qualitatively, the same results were obtained for an increase of the fractional charge of the hydrophilic A-segments. Naturally, the increase in τ leads to an increased Coulomb repulsion among the A-blocks. Logically, the opposite effects found at addition of simple salts reflects the reduction of the free energy cost of creating the electrostatic double layer in the corona region and in its closest vicinity.

Moreover, we observed that micelle formation was facilitated by a worsening of the solvent condition. The same appearance is known for uncharged block copolymers. The present finding is reasonable, since the effects of the solvent condition and the electrostatic interactions are to the leading order independent of each other.

The influence of the interaction between soluble segments and water on the thermodynamic stability of "hairy" micelle composed of uncharged diblock copolymers has previously been studied by Leermakers et al.[17] They found that with changing of solvent quality from good to Θ-solvent condition the region of stability extends to the larger aggregation numbers. This means that micelles form easier in the poorer solvent than in the good one, in agreement with our findings for charged soluble segments.

The stability conditions for a micelle with a large core and a thin uncharged corona (so-called "crew-cut" micelle) have been investigated also in the framework of the lattice mean-field theory.[16] The authors focused on the influence of the length of the hydrophobic block and the interaction parameter between segments of this block and water on the cmc. Lamellar structure was found as the preferred arrangement when the hydrophobic blocks became much larger than the hydrophilic ones. The reduced region of micellar structures obtained confirms the role of the repulsion among the hydrophilic segments for the stabilization of the micelles.

Finally, our predicted dependence on the salt concentration of the micellar sizes is in agreement with recent experimental works,[23,25] where a slight decrease of the thickness of the micellar corona with increasing salt concentration was found. In ref 23, it was also shown that the dependence of the micellar aggregation number on salt concentration can be described by two regimes. At low ϕ_s, the aggregation number increases with salt concentration, whereas at high ϕ_s it remains essentially constant, observations consistent with our data given in Figure 11.

5. Conclusions

On the basis of a lattice mean-field theory, we have analyzed the thermodynamic stability and the size of micelles formed by weakly charged diblock copolymers in a selective solvent. We have considered copolymers with a relatively short lyophobic block and a long and charged lyophilic block. Such architecture is known to give micelles with a relatively small aggregation number and an extended corona region.

Above the cmc, we have found that the volume fraction of the free diblock copolymers as well as the micellar aggregation number increases very slowly with increasing polymer concentration. The present study has qualitatively described how the cmc is affected by a number of system parameters. In particular, we found that (i) an increase of the length of the lyophilic block, (ii) an increase of the charge of the lyophilic block, and (iii) a reduction of the additional simple salt lead to an increase of the cmc and to smaller micellar aggregation numbers. Despite that, the micellar size, as monitored by the corona thickness, increases. Making the solvent poorer for the lyophilic block increases the aggregation number. On the basis of these observations, we conclude that, in addition to the core−solvent interaction promoting micelle formation, the repulsion in the corona region among the lyophilic blocks primarily arising from the nonlocal electrostatic contributions is another important factor regulating the aggregation number and the cmc.

In addition, we have also compared the dependences of the aggregation numbers, core radius, and corona thickness on the fractional charge, the length of the lyophilic block, and the salt concentration with scaling predictions. In the absence of added salt, predicted scaling dependencies for the weakly charged diblock copolymer were found to be consistent with the spherical Pincus brush regime. The dependencies on the salt concentration agreed well with scaling predictions. Such comparisons are however hampered by the fact that micelles are not often stable when a single parameter is varied over several orders of magnitude.

Acknowledgment. We thank Frans Leermakers for helpful suggestions. This work was financed by the Swedish Research Council for Engineering Science (TFR) and the Swedish National Research Council (NFR).

References and Notes

(1) *Developments in Block Copolymers*; Goodman, I., Ed; Applied Science: New York, 1982, Vol. 1; 1985; Vol. 2.
(2) Israelachvili, J. N. *Intermolecular and Surface Forces with Applications to Colloidal and Biological Systems*; Academic Press Inc. Ltd.: London, 1985.
(3) *Processing, Structure and Properties of Block Copolymers*; Folkes, M. J., Ed.; Elsever: New York, 1985.
(4) *Block Copolymers: Science and Technology*; Meier, D. J., Ed.; MMI Press Harwood Academic Publishers: New York, 1983.
(5) *Polymeric Surfactants*; Piirma, I., Ed.; Marcel Dekker: New York, 1992.
(6) Leibler, L.; Orland, H.; Wheeler, J. C. *J. Chem. Phys.* **1983**, *79*, 3550.
(7) Noolandi, J.; Hong, K. M. *Macromolecules* **1983**, *16*, 1443.
(8) Halperin, A.; Alexander, S. *Macromolecules* **1989**, *22*, 2403.
(9) Munch, M. R.; Gast, A. P. *Macromolecules* **1988**, *21*, 1360.
(10) Nagarajan, R.; Ganesh, K. *J. Chem. Phys.* **1989**, *90*, 5843.
(11) Fredrickson, G. H.; Leibler, L. *Macromolecules* **1989**, *22*, 1238.
(12) Zhulina, E. B.; Birshtein, T. M. *Vysokomol. Soedin. A* **1985**, *27*, 511. Birshtein, T. M.; Zhulina, E. B. *Polymer* **1989**, *30*, 170.
(13) Scheutjens, J. M. H. M.; Fleer, G. J. *J. Phys. Chem.* **1979**, *83*, 1619; **1980**, *84*, 178.
(14) Doi, M.; Edwards, S. F. *The Theory of Polymer Dynamics*; Clarendon Press: Oxford, U.K., 1986; Chapter 1.
(15) Leermakers, F. A. M.; Scheutjens, J. M. H. M. *J. Chem. Phys.* **1988**, *89*, 3264; **1988**, *89*, 6912; **1989**, *93*, 7417. Leermakers, F. A. M.; Scheutjens, J. M. H. M. *J. Colloid Interface Sci.* **1990**, *136*, 231. Leermakers, F. A. M.; Van der Schoot, P. P. A. M.; Scheutjens, J. M. H. M.; Lyklema, J. In *Surfactants in Solution*; Mittal, K. L., Ed.; Plenum Publishing Corp.: New York, 1990; Vol. 7.
(16) Van Lent, B.; Scheutjens, J. M. H. M. *Macromolecules* **1989**, *22*, 1931.
(17) Leermakers, F. A. M.; Wijmans, C. M.; Fleer, G. J. *Macromolecules* **1995**, *28*, 3434.
(18) Hill, T. L. *Thermodynamics of Small Systems*; Benjamin: New York, 1963 and 1964; Vols. 1 and 2.
(19) Linse, P. *Macromolecules* **1993**, *26*, 4437.
(20) Linse, P. *Macromolecules* **1994**, *27*, 6404.
(21) Hurter, P. N.; Scheutjens, J. M. H. M.; Hatton, T. A. *Macromolecules* **1993**, *26*, 5030.
(22) Wu, G.; Zhou, Z.; Chu, B. *Macromolecules* **1993**, *26*, 2117.
(23) Khougaz, K.; Astafieva, I.; Eisenberg, A. *Macromolecules* **1995**, *28*, 7135.
(24) Baines, F. L.; Armes, S. P.; Billingham, N. C.; Tuzar, Z. *Macromolecules* **1996**, *29*, 8151.
(25) Guenoun, P.; Davis, H. T.; Tirrel, M.; Mays, J. W. *Macromolecules* **1996**, *29*, 3965.
(26) Marko, J. F.; Rabin, Y. *Macromolecules* **1992**, *25*, 1503.
(27) Wittmer, J.; Joanny, J. F. *Macromolecules* **1993**, *26*, 2691.
(28) Dan, N.; Tirrel, M. *Macromolecules* **1993**, *26*, 4310.
(29) Shusharina, N. P.; Nyrkova, I. A.; Khokhlov, A. R. *Macromolecules* **1996**, *29*, 3167.
(30) Shusharina, N. P.; Saphonov, M. V.; Nyrkova, I. A.; Khalatur, P. G.; Khokhlov, A. R. *Ber. Bunsen-Ges. Phys. Chem.* **1996**, *100*, 857.
(31) Böhmer, M. R.; Evers, O. A.; Scheutjens, J. M. H. M. *Macromolecules* **1990**, 23, 2288.
(32) Israels, R. Thesis, Wageningen, 1994.
(33) van de Steeg, H. G. M.; Cohen Stuart, M. A.; de Keizer, A.; Bijsterbosch, B. *Langmuir* **1992**, *8*, 2538.
(34) Shubin, V.; Linse, P. *J. Phys. Chem.* **1995**, 99, 1285. Linse, P. *Macromolecules* **1996**, *29*, 326.
(35) Israels, R.; Leermakers, F. A. M.; Fleer, G. J.; Zhulina, E. B. *Macromolecules* **1994**, *27*, 3249.
(36) Wolterink, J. K.; Leermakers, F. A. M.; Fleer, G. J.; Koopal, L. K.; Zhulina, E. B.; Borisov, O. V. *Macromolecules* **1999**, *32*, 2365.
(37) Borisov, O. V.; Birshtein, T. M.; Zhulina, E. B. *J. Phys. II* **1991**, *1*, 521. Borisov, O. V.; Zhulina, E. B.; Birshtein, T. M. *Macromolecules* **1994**, *27*, 4795. Zhulina, E. B.; Borisov, O. V.; Birshtein, T. M. *J. Phys. II* **1992**, *2*, 63.
(38) Borisov, O. V. *J. Phys. II* **1996**, *6*, 1.
(39) Zhulina, E. B.; Borisov, O. V. *Macromolecules* **1996**, *29*, 2618.
(40) Borisov, O. V.; Zhulina, E. B. *Eur. Phys. J. B.* **1998**, *4*, 205.
(41) Shusharina, N. P.; Linse, P.; Khokhlov, A. R. *Macromolecules* **2000**, *33*, 3892.
(42) Flory, P. J. *Principles of Polymer Chemistry*; Cornell University Press: Ithaca, NY, 1953.
(43) Linse, P.; Björling, M. *Macromolecules* **1991**, *24*, 6700.
(44) Linse, P. *J. Phys. Chem.* **1993**, *97*, 13896.
(45) Borisov, O. V.; Zhulina, E. B., to be published.

MA0005567